First principles simulations of antiphase defects on the SP 90° partial dislocation in silicon

2006 J. Phys.: Condens. Matter 18 3735

(http://iopscience.iop.org/0953-8984/18/15/018)

INSTITUTE OF PHYSICS PUBLISHING JOURNAL OF PHYSICS: CONDENSED MATTER

J. Phys.: Condens. Matter **18** (2006) 3735–3744 doi:10.1088/0953-8984/18/15/018

First principles simulations of antiphase defects on the SP 90° partial dislocation in silicon

Alexander Valladares[1] **and A P Sutton**[2]

Materials Modelling Laboratory, Department of Materials, University of Oxford, OX1 3PH, UK

E-mail: avalladarm@servidor.unam.mx and a.sutton@imperial.ac.uk

Received 12 August 2005, in final form 31 January 2006
Published 30 March 2006
Online at stacks.iop.org/JPhysCM/18/3735

Abstract

We study the structure and energies of formation of antiphase defects on the single period (SP) 90° partial dislocation in silicon using a first principles density functional method. We consider two types of antiphase defect, the type first proposed by Hirsch (1980 *J. Microsc.* **118** 3) wholly inside the dislocation core, and another type that lies partly outside the core. Both types are stable and contain one atom which is threefold coordinated. Each of these atoms has a dangling hybrid which lies in a direction perpendicular to the dislocation line on the slip plane. We obtain values of 1.39 ± 0.03 eV and 1.41 ± 0.03 eV for the average formation energy of single antiphase defects of the inside and outside types, respectively. We have obtained, using a tight binding scheme, bandstructures corresponding to these two types of defect, and we find both of them to be associated with states in the gap and each dangling hybrid to contain one electron.

1. Introduction

The 90° partial is one of the most common types of dislocation found in silicon. Together with the 30° partial it is the dissociation product of perfect 60° dislocations (Hirth and Lothe 1982). It lies along ⟨110⟩ directions in {111} slip planes and it has a Burgers vector of the type $\frac{1}{6}\langle 112\rangle$. It is believed to have a reconstructed core (Hirsch 1985), and several possible reconstructions have been suggested. The two which have been shown by simulation to be stable (Bigger *et al* 1992, Bennetto *et al* 1997, Valladares and Sutton 2005a), are the single period (SP) and double period (DP) structures. In this work we focus on antiphase defects in the SP reconstruction.

The existence of antiphase defects was first proposed by Hirsch (1980) and they are expected to be a natural consequence of the SP reconstruction of dislocations. An antiphase

[1] Present address: Laboratorio Interdisciplinario, Departamento de Física, Facultad de Ciencias, UNAM, México DF, 04510, Mexico.

[2] Present address: Department of Physics, Imperial College London, Exhibition Road, London SW7 2AZ, UK.

defect is the boundary between regions on a given dislocation which are reconstructed in opposite senses. They can combine with pure kinks to form kink–antiphase defect complexes (Hirsch 1980, Bulatov *et al* 1995). The structure and mobility of these complexes can be very different from those of pure kinks. For the SP 90° partial, the complexes are the only stable kink defects (Valladares *et al* 1998, Valladares and Sutton 2005b). Antiphase defects have been considered in some cases to play an important role in the effect that donor and acceptor impurities have on the velocity of dislocations. According to Heggie and Jones (1983), they constitute the sites where double kink nucleation will occur preferentially, and this will affect the nucleation rate of kink pairs and therefore the velocity. Antiphase defects are thought in general to be associated with dangling bonds. However, to our knowledge no electron paramagnetic resonance (EPR) signals have been attributed to these defects on 90° partials, as distinct from other defects such as vacancies (Alexander and Teichler 1992).

In this work we study the structure, energies of formation and energy levels of these defects on the SP 90° partial in silicon using first principles methods.

2. Simulation method

We have used supercells and periodic boundary conditions. Each cell contained two 90° partials with opposite Burgers vectors separated by a ribbon of intrinsic stacking fault, i.e. a dislocation dipole. All cells contained 512 atoms with cell vectors $\frac{4}{2}[11\bar{2}]$, $\frac{2}{2}[11\bar{2}] + \frac{4}{3}[111] + \frac{1}{4}[1\bar{1}0]$ and $\frac{8}{2}[1\bar{1}0]$. The obliqueness of the cells was such that when repeated periodically they generated a quadrupolar lattice of dislocations (Bigger *et al* 1992). The partials in each cell had opposite senses of reconstruction, as required (Valladares and Sutton 2005b). We considered cells with straight defect-free 90° partials and cells containing a total of four antiphase defects, two on each partial, in order to satisfy the periodic boundary conditions.

To model the atomic interactions we used the Tersoff potential (Tersoff 1986) and a first principles density functional method. The Tersoff potential was employed to obtain relaxed structures of dislocations and antiphase defects which were used as input for the more accurate first principles relaxations. The parameter set used appeared in Tersoff (1988). This parameter set has been fitted to reproduce the three elastic constants of silicon, and the bond lengths and cohesive energies of real and hypothetical polytypes of silicon, so that the potential can better describe structures with different coordinations. Moreover, it gives results in good overall agreement with the density functional calculations of Bigger *et al* (1992) on the SP reconstructed 90° partial. All Tersoff relaxations were carried out using a molecular dynamics simulated annealing technique (Allen and Tildesley 1987) followed by conjugate gradients energy minimization (Press *et al* 1992).

The first principles calculations were carried out using the total energy code CETEP. The local density approximation was used for the exchange–correlation energy in the Perdew–Zunger form (Perdew and Zunger 1981). Nonlocal pseudopotentials (Rappe *et al* 1990, Lin *et al* 1993) with s and p components only were used for the ion cores. These were applied in the Kleinman–Bylander form (Kleinman and Bylander 1982) taking the p component as local and the s component as nonlocal and using a real space projection technique developed in King-Smith *et al* (1991). The occupied valence orbitals were expanded in a plane wave basis set with an energy cutoff of 96 eV, following Pérez *et al* (1995). In view of the large size of our supercells only the Γ point of the Brillouin zone was sampled. The total energy was minimized with respect to the electronic and ionic degrees of freedom, using a conjugate gradients method for the former and a variable metric method for the latter (Press *et al* 1992, Payne *et al* 1992). The relaxations were deemed complete when the forces on all atoms were below 0.1 eV Å^{-1}.

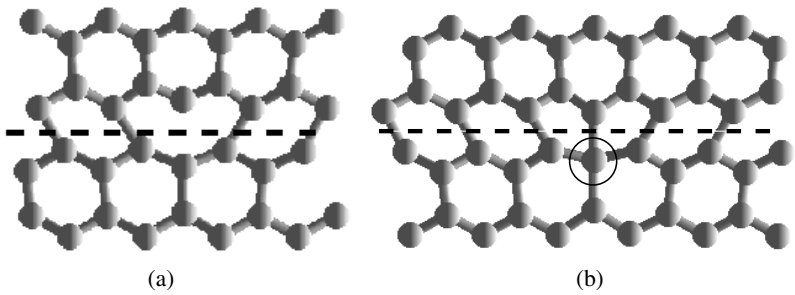

Figure 1. Types of antiphase defect on the SP 90° partial looking down on the (111) slip plane, as obtained with the Tersoff potential. (a) Structure originally proposed by Hirsch (1980). (b) Structure of a second type of antiphase defect containing one fivefold coordinated atom (encircled).

3. Results and discussion

We have found in our Tersoff simulations two different types of antiphase defect, shown in figures 1(a) and (b). The structure shown in figure 1(a) is the same as that originally proposed by Hirsch (1980). It contains an atom which is only threefold coordinated. Figure 1(b) shows the other structure we have obtained. Note that it contains an atom which is fivefold coordinated.

For each of these structures, we also have antiphase defects of the opposite 'sign'. Two antiphase defects of opposite sign on an otherwise defect-free dislocation will have the effect of leaving the reconstruction sense unaltered except in the segment between the defects, where it will be reversed.

We have constructed three 512-atom cells of the shape and size stated above, one with just two defect-free 90° partials and two cells with four antiphase defects each, one cell for each of the two antiphase defect structures. In the latter case, each partial contained two antiphase defects of opposite signs. We relaxed these cells first using the Tersoff potential, and then with the density functional code CETEP (Payne *et al* 1992).

3.1. Types of antiphase defects and structure

Two distinct antiphase defect structures were obtained from our first principles relaxations: the structure proposed by Hirsch and another structure obtained as a result of relaxing the cell containing the fivefold coordinated antiphase defects. The latter relaxed away from the structure obtained with the Tersoff potential. The fivefold coordinated atom moved upwards and bonded strongly with the atom above, leaving the atom immediately below threefold coordinated. This is the same structure as that obtained by Ewels *et al* (2000). However, these authors consider the structure to be that of a kink pair nucleated at an antiphase defect. We believe it is more appropriate to consider it an antiphase defect. Heggie and Jones (1983) proposed a mechanism consisting of a number of steps starting from a Hirsch antiphase defect and ending with a complex pair plus the Hirsch antiphase defect. The complex pair may then separate. One of the intermediate configurations corresponds to the structure shown in figure 3. In our view this should not be considered a kink pair because the constituent 'kinks' cannot separate before transforming into a pair of complexes plus another antiphase defect.

Figures 2 and 3 show the valence electronic charge density in electrons Å^{-3} in the slip plane for both types of antiphase defect.

Both structures contain an atom which is threefold coordinated. All other atoms are fourfold coordinated with strong covalent bonds between them. These bond charge densities

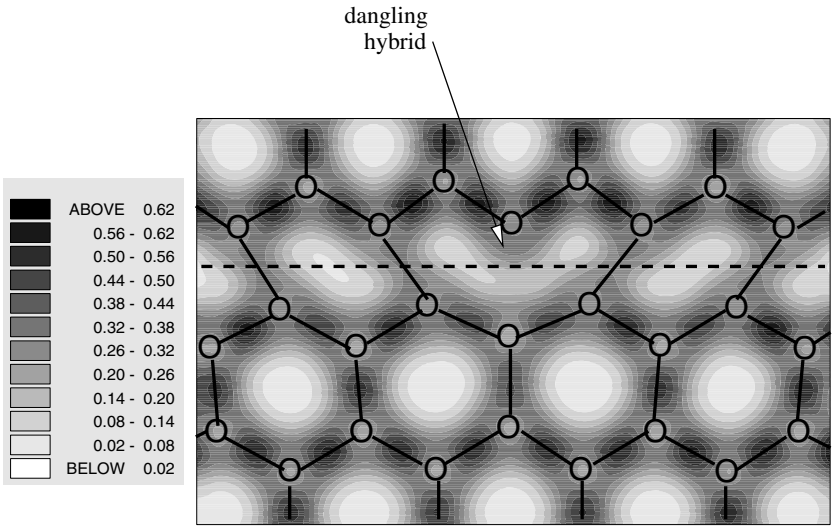

Figure 2. Valence electronic charge density in electrons Å^{-3} for an inside antiphase defect. The plane in which the charge density is shown lies midway between the two atomic planes that make up the whole atomic slip plane. Bonds in the dislocation core lie in a slightly different plane and therefore appear weaker. The circles correspond to atoms which lie either slightly above or below the plane of the figure. The broken line shows the dislocation line whereas the solid lines correspond to bonds. All atoms are fourfold coordinated with strong bonds between them, except one which is threefold coordinated. We see a dangling hybrid on this atom, pointing downwards.

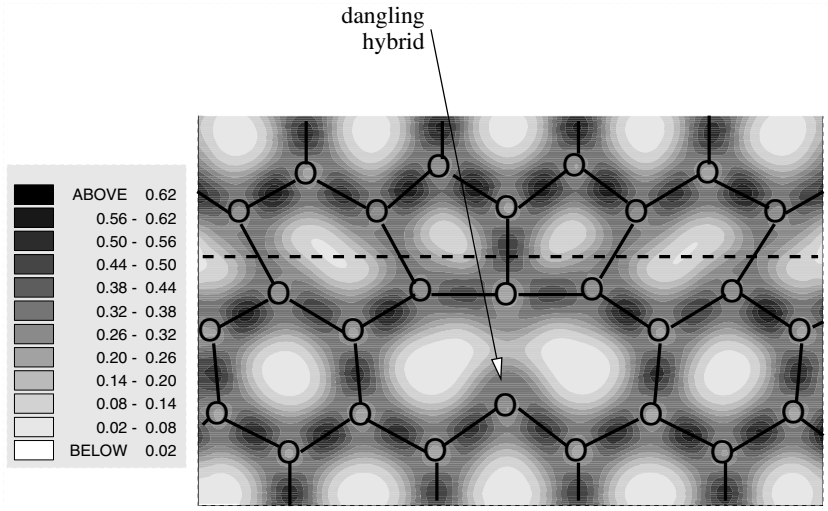

Figure 3. Same as figure 2 but for an outside antiphase defect. In this structure there is a different atom which is threefold coordinated. A dangling hybrid can be seen on this atom.

are comparable to those of bonds in the bulk. A dangling hybrid can be seen in each structure, with charge density lower than that of bonds, as expected. It is interesting that the antiphase defect of figure 3 has the dangling hybrid on an atom outside the dislocation core. For this reason we call the defect shown in figure 3 the outside antiphase defect and that shown in figure 2 the inside antiphase defect.

For both structures, the charge density plots for the antiphase defects of opposite sign are similar. Opposite sign antiphase defects are not related by symmetry and so there are four distinct types of antiphase defect.

3.2. Formation energies

The difference in total energies between the cell containing antiphase defects, with either structure, and the cell containing defect-free dislocations arises solely from the presence of antiphase defects. The stacking fault area is the same in all cells, as are the dislocation configurations, i.e. we always have straight dislocations. The relative senses of the dipolar lines of force (Valladares and Sutton 2005b) differ in the antiphase defect cells in comparison to the defect-free cell, and this may contribute to the energy difference. However, our use of opposite reconstruction senses for each pair of partials avoids bending of the dislocation lines and therefore we expect this contribution not to have a significant influence (Valladares and Sutton 2005b). Thus, the total energy difference is twice the energy of formation of an antiphase defect pair of opposite sign, for both structures.

We have obtained for an inside antiphase defect pair an energy of formation of 2.69 and 2.53 eV for an outside pair. Bandstructures associated with the cells were obtained (see below) using tight binding with an sp^3s^* basis. Since the average dispersion of the bands is 0.1 eV, we estimate that there is an error due to our k-point sampling of ± 0.05 eV in the formation energies of the antiphase defect pairs. Therefore, the average energy of formation of a single inside antiphase defect is 1.34 ± 0.03 eV, and for an outside antiphase defect it is 1.26 ± 0.03 eV. The fact that these two first principles values are close to each other is reasonable, since both structures contain one dangling hybrid.

Heggie *et al* (1993) calculated the formation energy of the inside antiphase defect using clusters and a local density functional method. They obtained 1.2 eV for a single inside antiphase defect. After increasing the cluster size and basis set per atom, this value increased to 1.4 eV (Ewels *et al* 2000). Nunes *et al* (1998), using tight binding and periodic boundary conditions, obtained a value of 1.45 eV for this defect. For the outside antiphase defect structure, Ewels *et al* (2000) obtained a value of 1.51, 0.11 eV higher than their energy for the inside antiphase defect. Unfortunately, there are no available experimental values for the energy of formation of antiphase defects on the 90° partial. We discuss the formation energies further in the next section.

3.3. Bandstructures

We have obtained bandstructures associated with the different first principles relaxed cells using an sp^3s^* tight binding scheme due to Vogl *et al* (1983). The Hamiltonian parameters have been fitted to the experimental bandstructure of silicon at high symmetry points. The inclusion of an excited s^* state reproduces the indirect band gap of this material and a good description of the valence and lower conduction bands is obtained. The length scaling of the hopping integrals has been taken to be proportional to $1/R^2$ and we have used a cutoff radius of 2.61 Å, which lies between first and second nearest neighbours in the diamond cubic structure. This cutoff has been chosen in order to have consistency with the first principles charge densities in terms of which atoms are bonded and which are not. The values of the Hamiltonian parameters can be found in Vogl *et al* (1983).

The bandstructure corresponding to the defect-free partials has already been discussed in Valladares and Sutton (2005b). The main feature is that the dislocations are associated only with shallow states above the valence band, the gap being essentially clear, which is consistent with the strong SP reconstruction.

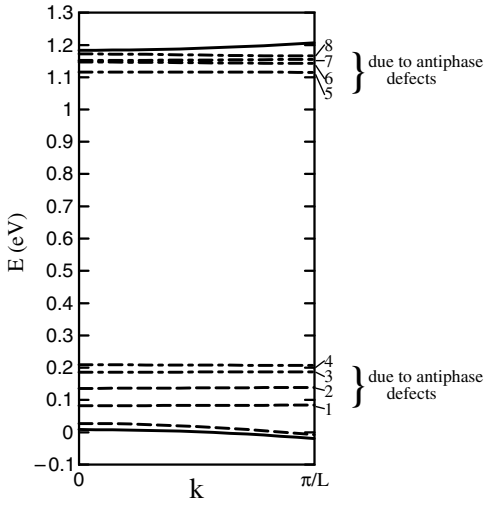

Figure 4. Projected bandstructure along the dislocation line, $[1\bar{1}0]$, of the first principles relaxed cell containing four inside antiphase defects. The solid lines correspond to the valence and conduction band edges of perfect silicon. The two types of broken line correspond to occupied (one dash) and unoccupied (long dash, short dash) bands associated with dislocations and antiphase defects. We have numbered these bands from 1 to 8.

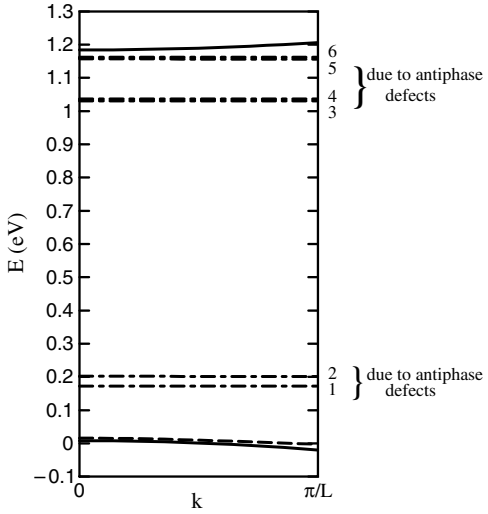

Figure 5. Same as figure 4 but for the cell containing four outside antiphase defects. We have numbered the states in the gap from 1 to 6.

Figures 4 and 5 show the projected bandstructures along the dislocation line direction associated with the cells containing inside and outside antiphase defects, respectively. The solid lines correspond to the valence and conduction band edges of perfect silicon while the dispersionless broken lines correspond to the antiphase defect bands.

We see that antiphase defects are associated with states above the valence band and below the conduction band. As in the case of defect-free dislocations, we have a very shallow band just above the valence band. But now we also have a series of deeper dispersionless states. We

have numbered these bands in order of increasing energy from 1 to 8 in figure 4, and from 1 to 6 in figure 5. To understand their origin, we have examined the eigenvectors corresponding to each of the Γ point eigenvalues. We consider the Γ point to be sufficient since these bands show virtually no dispersion.

First let us consider figure 4. At 0 K, bands up to and including bands 1 and 2 are filled with two electrons in each state allowing for spin. All states lying above are unoccupied. We have used two types of broken line to differentiate between occupied and unoccupied bands.

The components of the eigenvector associated with band 1 indicate that this state is localized on two of the four antiphase defects, these two defects lying directly opposite each other, one on each partial. This corresponds to a bonding combination of these two dangling hybrids on each of the threefold coordinated atoms, lying in the slip plane and pointing in a direction perpendicular to the dislocation line. The lack of dispersion of the band is consistent with these states being localized along the dislocation line.

Turning to band 2, the dominant atomic state coefficients now correspond to the threefold coordinated atoms on the other two antiphase defects. Band 2 states correspond to a bonding combination of these two dangling hybrids lying in the slip plane and pointing in a direction perpendicular to the dislocation line.

Interestingly, bands 1 and 2 are not degenerate and the atomic state coefficients of all four threefold coordinated atoms, although similar, are not identical. This is partly because the antiphase defects are not all identical, since some have opposite signs. But also, the existence of an antiphase defect on an SP 90° partial means that the reconstruction sense changes in $1\frac{1}{2}$ SP periods. Since we have 8 SP periods in our cells and two antiphase defects on each partial, the separation between the centres of antiphase defects is $3\frac{1}{2}$ periods followed by $4\frac{1}{2}$, $3\frac{1}{2}$, etc, when we repeat the cell. This renders otherwise equivalent antiphase defects slightly different in terms of the environment that surrounds them.

Since the coefficients associated with the threefold coordinated atoms in each pair of antiphase defects are comparable in magnitude, and since the bonding states constituting bands 1 and 2 are each occupied with two electrons, we conclude that there is one electron localized at each antiphase defect. This is consistent with figure 2, which shows the charge density associated with the dangling hybrid to be less than the charge densities of bonds between neighbouring atoms.

The eigenstates of bands 3 and 4 correspond to unoccupied anti-bonding combinations of pairs of the same dangling hybrids that give rise to bands 1 and 2, respectively. The bonding–anti-bonding splittings of bands 1 and 3 and of bands 2 and 4 are about 0.1 eV. Examining the atomic state coefficients of eigenstates associated with unoccupied bands 5, 6, 7 and 8 in figure 4, we find these eigenstates are localized on one or more antiphase defects and involve primarily fourfold coordinated atoms.

Now let us consider the bandstructure in figure 5. Now all six dispersionless bands are unoccupied. The dominant atomic state coefficients of the eigenstates of band 1 belong to threefold coordinated atoms in two of the four antiphase defects. These eigenstates are associated with anti-bonding combinations of the two dangling hybrids. Similarly for band 2 the eigenstates are associated with anti-bonding combinations of the other two antiphase defects. The nondegeneracy of these two bands arises for the same reasons as for bands 1 and 2 of figure 4. For bands 3, 4, 5 and 6, the eigenvectors indicate that the states are localized on antiphase defects and involve only atoms which are fourfold coordinated.

Turning to the occupied states, analysis of the eigenvectors associated with the highest bands below band 1, all lying in the valence band or just above, yields the following. There are two states with virtually no dispersion, not shown in figure 5, lying approximately 0.1 eV below the top of the valence band, which are localized on antiphase defects. The lower of

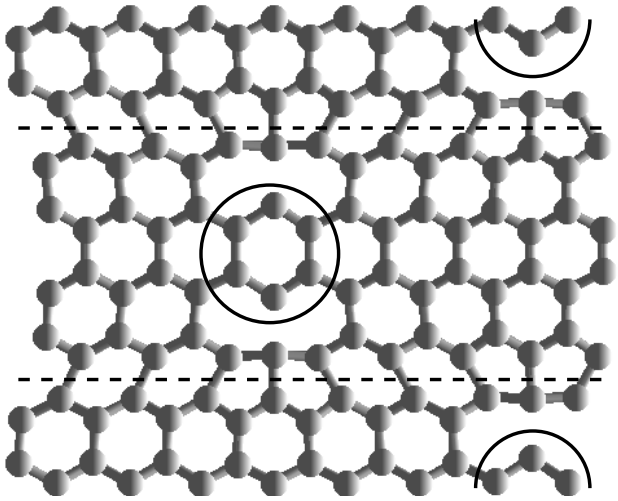

Figure 6. Relaxed atomic structure of the cell containing outside antiphase defects looking down on the slip plane. Note how the threefold coordinated atoms in pairs of defects directly opposite each other form part of the same six-membered rings (circled).

the two is localized on the same two defects as band 1, while the other is localized on the remaining two defects. The eigenstates of these two bands are bonding state combinations of the corresponding antiphase defect dangling hybrids. These states are therefore resonances in the valence band.

The reason why these eigenstates are not in the gap but in the valence band, even though they correspond to dangling hybrids, is likely to be the following. The structure of the antiphase defects outside the core and the size of our cell are such that the threefold coordinated atoms on defects directly opposite each other form part of the same six-membered ring lying in the slip plane. This is shown in figure 6.

By contrast the dangling hybrids in inside antiphase defects are further apart. As a consequence the bonding–anti-bonding splitting is about 0.3 eV for the dangling hybrids in the outside defects and this depresses the energy of the bonding combination into the valence band.

The question arises as to whether the existence of the outside antiphase defects is an artefact of their proximity and of pairs of threefold coordinated atoms forming part of the same six-membered rings. This is not the case. We have performed first principles relaxations of cells containing double kink defects (Valladares and Sutton 2005b). In the relaxation of a cell containing fivefold and threefold coordinated kinks, these defects transformed spontaneously into complexes plus antiphase defects. Both types of antiphase defect were obtained at the end of this relaxation and the environment of the outside antiphase defect is completely different in this case, indicating that its existence is not caused by the particular atomic configuration shown in figure 6. Figure 7 illustrates this.

Our analysis of figure 5 shows that there is essentially one electron in each dangling hybrid. This is consistent with the charge density plot in figure 3, where we see a dangling hybrid, its charge density being lower than that of the surrounding bonds.

The positions of the occupied states of the two types of antiphase defect are consistent with the inside defect having a slightly higher energy than the outside defect.

However, the splittings for the bonding and anti-bonding combinations of dangling hybrids associated with the inside and outside antiphase defects are 0.1 and 0.3 eV, respectively. This

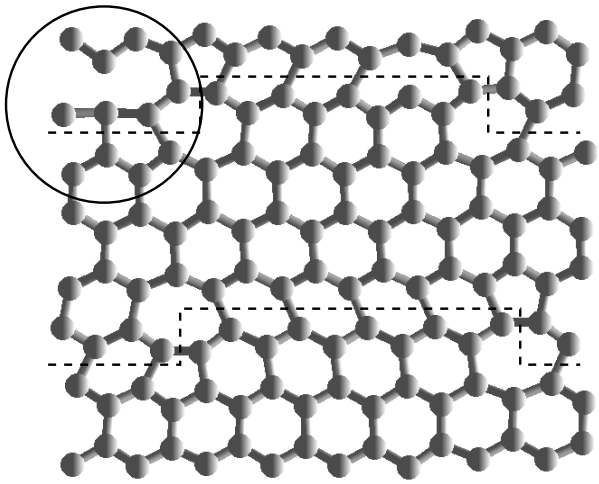

Figure 7. Final first principles relaxed atomic structure of a cell originally containing fivefold and threefold coordinated kinks looking down on the slip plane. At the end of the relaxation there are complexes and both types of antiphase defect. Note how the environment of the outside antiphase defect (circled) is completely different in this case.

suggests that the formation energy we obtained for isolated inside and outside defects could be too low by 0.05 and 0.15 eV, respectively. In that case our formation energies become 1.39 ± 0.03 eV and 1.41 ± 0.03 eV for the inside and outside antiphase defects, respectively. These values compare reasonably well with those obtained by Ewels *et al* (2000) and by Nunes *et al* (1998).

We have calculated the tight binding atomic charges in the two antiphase defect cells. In both cells, all atoms are almost neutral, the maximum charge on any one atom being about ± 0.2–0.3 electrons. These maximum values are comparable to the maximum atomic charges we obtained when calculating the bandstructure associated with the motion of complexes on the 90° partial using the same tight binding scheme but self-consistently (Valladares and Sutton 2005b). Hence, we do not consider self-consistency to be essential in the present simulations since atoms are already close to neutral.

Heggie *et al* (1991) obtained the energy levels of the inside antiphase defects from their density functional cluster calculations. A comparison with our results is difficult because the gap they calculated is so large. They find these defects to be associated with a state 1.5 eV above the valence band, which lies in the middle of their gap. No comparison of the precise placement of the states is possible.

4. Conclusions

The antiphase defect structure proposed by Hirsch (1980), in which there is a dangling hybrid inside the dislocation core, has been found to be stable by first principles simulation. Another structure of the antiphase defect, considered by Ewels *et al* (2000) in a different context, is also found to be stable. In the latter configuration the dangling hybrid is outside the dislocation core. Both types of antiphase defect are associated with states in the gap. An analysis of the occupation of these states indicates that each dangling hybrid contains one electron. We have obtained a value of 1.39 ± 0.03 eV for the average energy of formation of a single inside

antiphase defect and 1.41 ± 0.03 eV for an outside defect. We conclude that the errors associated with our calculations are such that we cannot discriminate between the formation energies of the inside and outside antiphase defects.

Acknowledgments

We would like to thank Dr James A White for his help with the CETEP code. We also thank Drs Andrew Horsfield and Steven Kenny for helping us with the Plato code. AV is grateful to DGAPA and Facultad de Ciencias, Universidad Nacional Autónoma de México, for support.

References

Alexander H and Teichler H 1992 *Materials Science and Technology* vol 4, ed R W Cahn, P Haasen and E J Kramer (Cambridge: VCH Weinheim)
Allen M P and Tildesley D J 1987 *Computer Simulation of Liquids* (Oxford: Clarendon)
Bennetto J, Nunes R W and Vanderbilt D 1997 *Phys. Rev. Lett.* **79** 245
Bigger J R K, Mc Innes D A, Sutton A P, Payne M C, Stich I, King-Smith R D, Bird D M and Clarke L J 1992 *Phys. Rev. Lett.* **69** 2224
Bulatov V V, Yip S and Argon A S 1995 *Phil. Mag.* A **72** 453
Ewels C P, Leoni S, Heggie M I, Jemmer P, Hernandez E, Jones R and Briddon P R 2000 *Phys. Rev. Lett.* **84** 690
Heggie M and Jones R 1983 *Inst. Phys. Conf. Ser.* **67** 45
Heggie M, Jones R and Umerski A 1991 *Phil. Mag.* A **63** 571
Heggie M, Jones R and Umerski A 1993 *Phys. Status Solidi* a **138** 383
Hirsch P B 1980 *J. Microsc.* **118** 3
Hirsch P B 1985 *Mater. Sci. Technol.* **1** 666
Hirth J P and Lothe J 1982 *Theory of Dislocations* (Malabar, FL: Krieger)
King-Smith R D, Payne M C and Lin J S 1991 *Phys. Rev.* B **44** 13063
Kleinman L and Bylander D M 1982 *Phys. Rev. Lett.* **48** 1425
Lin J S, Qteish A, Payne M C and Heine V 1993 *Phys. Rev.* B **47** 4174
Nunes R W, Bennetto J and Vanderbilt D 1998 *Phys. Rev.* B **57** 10388
Payne M C, Teter M P, Allan D C, Arias T A and Joannopoulos J D 1992 *Rev. Mod. Phys.* **64** 1045
Perdew J P and Zunger A 1981 *Phys. Rev.* B **23** 5048
Pérez R, Payne M C and Simpson A D 1995 *Phys. Rev. Lett.* **75** 4748
Press W H, Teukolsky S A, Vetterling W T and Flannery B P 1992 *Numerical Recipes in Fortran* (Cambridge: Cambridge University Press)
Rappe A M, Rabe K M, Kaxiras E and Joannopoulos J D 1990 *Phys. Rev.* B **41** 1227
Tersoff J 1986 *Phys. Rev. Lett.* **56** 632
Tersoff J 1988 *Phys. Rev.* B **38** 9902
Valladares A and Sutton A P 2005a *J. Phys.: Condens. Matter* **17** 7547
Valladares A and Sutton A P 2005b First principles simulations of kink defects on the SP 90° partial dislocation in silicon *Prog. Mater. Sci.* submitted
Valladares A, White J A and Sutton A P 1998 *Phys. Rev. Lett.* **81** 4903
Vogl P, Hjalmarson H P and Dow J D 1983 *J. Phys. Chem. Solids* **44** 365